International Journal of Basic and Applied Chemical Sciences ISSN: 2277-2073 (Online)
An Open Access, Online International Journal Available at http://www.cibtech.org/jcs.htm
2018 Vol. 8(2) April-June, pp.1-19/Shukla et al.

Research Article

SYNTHESIS, COMPUTATIONAL AND SPECTROSCOPIC STUDIES OF SOME THIOUREA SCHIFF BASE METAL COMPLEXES AND ITS APPLICATIONS AS CORROSION INHIBITION, CATALASE LIKE ACTIVITY AND ANTIBACTERIAL SCREENING

***S. N. Shukla, Pratiksha Gaur, Preeti Vaidya, Bhaskar Chaurasia, Sangeeta Jhariya, Dimple Dehariya**
Coordination Chemistry Research Lab, Department of Chemistry, Government Science College, Jabalpur (M.P.) 482001, India
**Author for Correspondence*

ABSTRACT

Four mononuclear complexes *viz* [M(BENZONTHURA)(H_2O)$_2$] and [Fe(BENZONTHURA)(H_2O) (Cl)] where **BENZONTHURA** = (1E,3E)-1,3-bis(2-hydroxy-1,2-diphenylethylidene)thiourea and M = Mn(II), Co(II), Ni(II), were prepared and fully characterized using elemental analyses, FT-IR, molar conductivity, magnetic susceptibility, ESI-MS, electronic spectra, ^{1}H-NMR and ^{13}C-NMR spectroscopy. Computational studies were performed using DFT calculations at B3LYP/6-311+G(d,p) and LANL2DZ level of theory. Additionally, molecular electrostatic potential map (MEP), HOMO, LUMO, NBO and Mulliken charge analysis were also been performed. Spectroscopic characterization and DFT study proposed a distorted octahedral structure of complex **1-4**. Corrosion inhibition effect of ligand and complexes on mild steel in 0.5 M HCl solution for 24 h, 48 h, and 72 h was studied by using weight loss techniques. The results of anticorrosion activity of **BENZONTHURA** and complex **1-4** were found in the order: **BENZONTHURA > 4 > 3 > 1 > 2**. *In vitro*, bio-mimetic catalase activity and antibacterial activity of the synthesized compounds show that complexes were more potent than the **BENZONTHURA**. MIC of complex **1-4** shows that complex **4** is more active than other complexes even at a lower concentration.

Keywords: *Tetradentate Schiff base; Bio-mimetic; Catalase activity; DFT study; Corrosion inhibition; Antibacterial activity.*

.

INTRODUCTION

Thiourea derived Schiff base ligands are versatile organic molecules which are capable of coordinating with metal ions and binding with biological targets to form stable complexes (Arslan *et. al.*, 2009). These organic compounds usually contain heteroatoms (N, O, and S) as well as double bonds or aromatic rings in their molecular structures. Owing to this, these kind of ligands are useful as corrosion inhibitors (Guo *et. al.*, 2017), antibacterials (Bielenica *et. al.*, 2015), antioxidants (Walpole *et al.*, 1998), anticancer agents (Rauf *et. al.*, 2016) and can be used to prevent lung injury induced by ROS (Lai *et. al.*, 1998). Thiourea is also known to be a powerful scavenger of $O_2^{\cdot-}$ and $OH^{\cdot}$ (Fox *et. al.*, 1993).

It is well known that certain reactive oxygen species (ROS) including superoxide radical anion ($O_2^{\cdot-}$) and hydroxyl radical ($OH^{\cdot}$) which are generated during metabolic processes in biological systems damage biomolecules including DNA, proteins, lipids etc and cause different diseases of vital organs of the human body (Halliwell *et. al.*, 1984; Ray *et. al.*, 1999). For example, it has been found that $O_2^{\cdot-}$ and $OH^{\cdot}$ plays crucial roles in cardiovascular and neurodegenerative diseases as well as in cancer (Collin *et. al.*, 2007; Kadiiska *et. al.*, 1997). Ultraviolet radiation, ozone (O_3), tobacco smoke, inflammatory cytokines and chemotherapeutic drugs are exogenous sources that are responsible for the generation of cellular ROS (Thannickal *et. al.*, 2000). It is also known that $O_2^{\cdot-}$ and $OH^{\cdot}$ can be scavenged by the enzymes superoxide dismutase (SOD), catalase and glutathione peroxidise efficiently. However, catalase catalyzes disproportion of H_2O_2 into H_2O and O_2 (Brazier *et. al.*, 2008). Transition metals such as manganese, iron, cobalt, and nickel are present in the active site of the various metalloenzymes can also compete for binding sites with other cations of comparable size, making concentration and selection regulation necessary for cell life (Valdez *et al.*, 2014). It is also well documented that thiourea based ligands and their metal complexes display a wide range of antibacterial activity against various harmful bacterial cells (Zhang *et al.*, 1998).

On the other hand, the ability of thiourea and benzoin Schiff base ligands to form stable complexes closely packed in the coordination sphere of metal ion introduces another class of compounds for corrosion inhibition. A few recent reports indicate that the Schiff base ligands and their metal complexes show good corrosion inhibition efficiency (Singh *et. al.*, 2013).

In view of a number of cited literature, it is highly desirable that structures and properties of these molecules are to be studied in detail especially for their reactions related to the medicinal and biological aspects. The present study focuses upon exploring anticorrosive properties, bio-mimetic catalase-like activity and antibacterial activity of the resulting compounds.

MATERIALS AND METHODS

All the chemicals and solvents were used in A.R. grade. Thiourea, benzoin, sodium hydroxide, manganese(II) chloride, iron(III) chloride, cobalt(II) chloride, and nickel(II) chloride (E. Merck) were purchased from the market and used as received. Analytical reagent grade methyl alcohol, ethyl alcohol, (distilled before use) acetonitrile, acetone, dimethylformamide, dimethylsulphoxide, hydrogen peroxide, and hydrochloric acid (E. Merck) used as received. Mueller Hinton Agar, Nutrient Agar (Himedia), dry yeast, mild steel, and emery papers were purchased from the market and used as received. Elemental analysis was estimated on EuroVector E 3000 Elemental Analyser and metal contents were analyzed gravimetrically by the literature procedure (Jeffery *et al.*, 1989). Conductivity measurements were carried out in DMSO at 25 °C on an EI -181 conductivity bridge with dipping type cell. ESI-MS spectra were recorded on Agilent - 6520(Q-TOF) mass spectrometer. FT-IR spectra were recorded in KBr pellets on Shimadzu-8400 PC spectrometer. Electronic absorption spectra were recorded in the range 800-200 nm with an EI-2371 double beam spectrophotometer equipped with a PC. Guoy's method was employed for measurement of magnetic susceptibility. ^{1}H-NMR and the ^{13}C-NMR spectrum were recorded in DMSO-d6 on a Bruker Avance 400 (FT NMR) spectrophotometer (400 MHz).

Synthesis of ligand and complexes

Synthesis of (1E,3E)-1,3-bis(2-hydroxy-1,2-diphenylethylidene)thiourea; (BENZONTHURA)

Benzoin (4.24 g, 0.02 mol) dissolved in 15 mL ethanol was added to a solution of thiourea (0.76 g, 0.01 mol) dissolved in 15 mL ethanol in a flat bottom flask. The resulting mixture was stirred initially for 1 h and thereafter refluxed for 6 h in an inert atmosphere. Progress of the reaction was monitored by TLC. Off-white crystalline solid was obtained after cooling the mixture, which was filtered and recrystallized from hot ethanol to yield off-white crystals. These crystals were dried over anhydrous calcium chloride in a desiccator under vacuum. Colour = off-white, Yield: 4.35 g (87.01 %), m. p. = 212 ºC, Anal. Calc. formula $\mathbf{C_{29}H_{24}N_2O_2S}$ (Mτ = 464.58): C, 74.87; H, 5.21; N, 6.03. Found: C, 74.80; H, 5.19; N, 5.99. Selected infrared absorption (KBr, cm^{-1}): ν(O-H) 3356(w), ν(C=N)$_{imine}$ 1602(m), ν(C-O) 1255(s), ν(C=S) 773(s). Electronic spectra (λ_{max} in nm, ε in L mol^{-1} cm^{-1}) in DMF: 320(4335), 240(1887). ^{1}H-NMR spectra (δ value in ppm) in DMSO-d6: δ(Ar-H) 7.198(t, 1H), 7.235(t, 1H), 7.241(t, 1H), 7.280(d, 1H), 7.317(d, 1H), 7.335(d, 1H), 7.338(d, 1H), 7.346(t, 1H), 7.402(t, 1H), 7.420(t, 1H), 7.424(t, 1H), 7.439(t, 1H), 7.459(t, 1H), 7.475(t, 1H), 7.531(t, 1H), 7.534(t, 1H), 7.618(d, 1H), 7.910(d, 1H), 7.973(d, 1H), 7.976(d, 1H), 7.981(d, 1H). ^{13}C-NMR spectra (δ value in ppm): δ(C=S)$_{thione}$ 199.21, δ(C=N)$_{imine}$ 183.88, δ(C-O) 164.85, δ(Ar-C) 126.93-129.60, 132.25-139.70. ESI-Mass spectra, m/z: $[C_7H_7O + H^+]^+$ = 108.0340, $[C_{14}H_{12}NO + H^+]^+$ = 211.0762, $[C_{15}H_{21}NOS + H^+]^+$ = 255.0807, $[C_{22}H_{17}N_2OS + H^+]^+$ = 358.1068, $[C_{29}H_{24}N_2O_2S + H^+]^+$ = 465.1680, Mτ =464.58.

Synthesis of [Mn(BENZONTHURA)(H$_2$O)$_2$]; complex ***1***

Recrystallized ligand BENZONTHURA (0.464 g, 0.001 mol) dissolved in 25 mL ethanol was added to $MnCl_2{\cdot}4H_2O$ (0.161 g, 0.001 mol) in 15 mL ethanol in a two neck flat bottom flask. The resulting reaction mixture was stirred for 1 h in an inert atmosphere. A brown precipitate was obtained after refluxing the reaction mixture for 15 h. The precipitate obtained was filtered, washed several times with acetone, recrystallized from hot ethanol and dried in a desiccator over anhydrous calcium chloride under vacuum. Colour = brown, Yield: 0.399g (63.73 %), m.p. > 300 ºC, Anal. Calc. formula **$C_{29}H_{26}MnN_2O_4S$** (Mτ = 553.53): C, 62.93; H, 4.73; N, 5.06; Mn, 9.93. Found: C, 62.90; H, 4.69; N, 5.02; Mn, 9.89. μ_{eff} = 5.27 B.M. Molar conductance Λ_m at 25 °C ($\Omega^{-1}cm^2mol^{-1}$): 12 in DMSO. Selected infrared absorption (KBr, cm^{-1}): $\nu(H_2O)_{coordinated\ water}$ 3483(w), $\nu(C{=}N)_{imine}$ 1581(m), ν(C-O) 1290(s), $\gamma(H_2O)$ 832(s), ν(C=S) 756(m), ν(M-O) 589(s), ν(M-N) 476 (m). Electronic spectra (λ_{max} in nm, ε in L mol^{-1} cm^{-1}) in DMF: 720 (132), 640 (111), 580 (142), 360 (1237), 240 (299). ESI-Mass spectra, m/z: $[C_{14}H_{11}NO + H^+]^+$ = 210.1186, $[C_{15}H_{15}MnNO_3S]^+$ = 344.0277, $[C_{29}H_{22}N_2O_2S + 3H^+]^+$ = 465.2447, $[C_{29}H_{22}MnN_2O_2S + H^+]^+$ = 518.3091, $[C_{29}H_{24}MnN_2O_2S + H^+]^+$ = 536.0970, $[C_{29}H_{26}MnN_2O_4S + H^+]^+$ = 554.1057, Mτ = 553.53.

Synthesis of [Fe(BENZONTHURA)(H_2O)(Cl)]; complex **2**

Recrystallized Schiff base BENZONTHURA (0.464 g, 0.001 mol) dissolved in 25 mL ethanol was added to $FeCl_3$ (0.162 g, 0.001 mol) in 15 mL ethanol in a two neck round bottom flask. The resulting reaction mixture was stirred for 1 h in an inert atmosphere. A brown precipitate was obtained after refluxing the reaction mixture for 12 h. The precipitate obtained was filtered, washed several times with acetone, recrystallized from hot ethanol and dried in a desiccator over anhydrous calcium chloride under vacuum. Colour = brown, Yield: 0.378 g (60.38 %); m.p. > 300 ºC; Anal Calc. formula **$C_{29}H_{24}FeN_2O_3SCl$** (Mτ = 571.88): C, 60.91; H, 4.23; N, 4.90; Fe, 9.77. Found: C, 60.88; H, 4.20; N, 4.87; Fe, 9.73. μ_{eff} = 5.59 B.M. Molar conductance Λ_m at 25 °C ($\Omega^{-1}cm^2mol^{-1}$): 11 in DMSO. Selected infrared absorption (KBr, cm^{-1}): $\nu(H_2O)_{coordinated\ water}$ 3473(w), $\nu(C{=}N)_{imine}$ 1586(s), ν(C-O) 1289(s), $\gamma(H_2O)$ 836(s), ν(C=S) 758(s), ν(M-O) 582(s), ν(M-N) 465(s), ν(M-Cl) 403(m). Electronic spectra (λ_{max} in nm, ε in L mol^{-1} cm^{-1}) in DMF: 720 (19), 520 (25), 480 (19), 340 (540), 220 (345). ESI-Mass spectra, m/z: $[C_{14}H_{11}NO + H^+]^+$ = 210.1545, $[C_{15}H_{13}FeNO_2SCl]^+$ = 361.9715, $[C_{29}H_{22}N_2O_2S + 3H^+]^+$ = 465.1456, $[C_{29}H_{22}FeN_2O_2S + H^+]^+$ = 519.0891, $[C_{29}H_{24}FeN_2O_3S + H^+]^+$ = 537.0866, $[C_{29}H_{22}FeN_2O_2SCl + H^+]^+$ = 554.0441, $[C_{29}H_{24}FeN_2O_3SCl + H^+]^+$ = 572.0569, Mτ = 571.88.

Synthesis of [Co(BENZONTHURA)(H_2O)$_2$]; complex **3**

Recrystallized ligand BENZONTHURA (0.464 g, 0.001 mol) dissolved in 25 mL ethanol was added to $CoCl_2{\cdot}6H_2O$ (0.237 g, 0.001 mol) in 15 mL ethanol in a two neck round bottom flask. The resulting reaction mixture was stirred for 1 h in an inert atmosphere. A yellowish brown precipitate was obtained after refluxing the reaction mixture for 15 h. The solid obtained was filtered, washed several times with acetone, recrystallized from hot ethanol and dried in a desiccator over anhydrous calcium chloride under vacuum. Colour = yellowish brown, Yield: 0.449 g (64.05 %); m.p. > 300 ºC; Anal Calc. formula **$C_{29}H_{26}CoN_2O_4S$** (Mτ = 557.53): C, 62.47; H, 4.70; N, 5.02; Co, 10.57. Found: C, 62.40; H, 4.68; N, 5.00; Co, 10.54. μ_{eff} = 4.02 B.M. Molar conductance Λ_m at 25 °C ($\Omega^{-1}cm^2mol^{-1}$): 14 in DMSO. Selected infrared absorption (KBr, cm^{-1}): $\nu(H_2O)_{coordinated\ water}$ 3488(w), $\nu(C{=}N)_{imine}$ 1578(s), ν(C-O) 1275(m), $\gamma(H_2O)$ 830(s), ν(C=S) 757(w), ν(M-O) 585(s), ν(M-N) 462(m). Electronic spectra (λ_{max} in nm, ε in L mol^{-1} cm^{-1}) in DMF: 788 (22), 740 (32), 550 (19), 380 (1015), 240 (456). ESI-Mass spectra, m/z: $[C_{14}H_{11}NO + H^+]^+$ = 210.0909, $[C_{15}H_{15}CoNO_3S]^+$ = 348.0156, $[C_{29}H_{22}N_2O_2S + 3H^+]^+$ = 465.0466, $[C_{29}H_{22}CoN_2O_2S + H^+]^+$ = 522.0812, $[C_{29}H_{24}CoN_2O_3S + H^+]^+$ = 540.0812, $[C_{29}H_{26}CoN_2O_4S + H^+]^+$ = 558.0963, Mτ = 557.53.

Synthesis of [Ni(BENZONTHURA)(H_2O)$_2$]; complex **4**

Recrystallized ligand BENZONTHURA (0.464 g, 0.001 mol) dissolved in 25 mL ethanol was added to $NiCl_2{\cdot}6H_2O$ (0.237 g, 0.001 mol) in 15 mL ethanol in a two neck round bottom flask. The resulting reaction mixture was stirred for 1 h in an inert atmosphere. A green precipitate was obtained after refluxing the reaction mixture for 15 h. The precipitate obtained was filtered, washed several times with acetone, recrystallized from hot ethanol and dried in a desiccator over anhydrous calcium chloride under vacuum. Colour = green, Yield: 0.471 g (67.18 %); m.p. > 300 ºC; Anal Calc. formula **$C_{29}H_{26}NiN_2O_4S$** (Mτ = 557.29): C, 62.50; H, 4.70; N, 5.03; Ni, 10.53. Found: C, 62.47; H, 4.68; N, 5.00; Ni, 10.50. μ_{eff} = 2.99 B.M. Molar conductance Λ_m at 25 °C ($\Omega^{-1}cm^2mol^{-1}$): 16 in DMSO. Selected infrared absorption

(KBr, cm^{-1}): $\nu(H_2O)_{\text{coordinated water}}$ 3475(w), $\nu(C{=}N)_{\text{imine}}$ 1584(s), ν(C-O) 1280(s), $\gamma(H_2O)$ 838(s), ν(C=S) 751(m), ν(M-O) 580(m), ν(M-N) 460(m). Electronic spectra (λ_{max} in nm, ε in L mol^{-1} cm^{-1}) in DMF: 580 (55), 420 (48), 340 (1023), 240 (444). ESI-Mass spectra, m/z: $[C_{14}H_{11}NO + H^+]^+$ = 210.0912, $[C_{15}H_{15}NiNO_3S]^+$ = 347.0150, $[C_{29}H_{22}N_2O_2S + 3H^+]^+$ = 465.1450, $[C_{29}H_{22}NiN_2O_2S + H^+]^+$ = 521.0722, $[C_{29}H_{24}NiN_2O_3S + H^+]^+$ =539.0925, $[C_{29}H_{26}NiN_2O_4S + H^+]^+$ = 558.0860, Mτ = 557.29.

DFT calculations

The theoretical calculations were performed using GaussView molecular visualization program and Gaussian 09W program package (Frisch *et al.,* 2009). The molecular structure of ligand BENZONTHURA and complex 1-4 were fully optimized using the DFT approach. The B3LYP method with 6-31+G(d,p) basis set was used for all atoms of BENZONTHURA and LanL2DZ method was used for complex 1-4. The charge distribution on the atomic sites was computed using natural bond orbital (NBO) and Mulliken charge. Distribution of electronegative and electropositive atoms over the molecule was presented by the molecular electrostatic potential (MEP) maps (Becke, 1988; Lee *et al.*, 1988).

Anticorrosion activity

The anticorrosion activity of ligand BENZONTHURA and complex 1-4 was done by weight loss measurement method. The mild steel specimens cut into 3 × 4 × 0.05 cm^3 were abraded successively with different grades of emery paper, washed with distilled water, cleaned with acetone, dried, weighed and kept in a moisture free atmosphere. The corrosive media, 0.5 M of HCl was prepared by dilution of analytical grade HCl of predetermined normality with triple distilled water. Anticorrosive solutions were prepared by dissolving 50 ppm of each BENZONTHURA and complex 1-4 in 5 mL DMSO was added in electrolyte HCl at room temperature. Immerse the steel specimens in prepared solutions. The specimens were taken out from electrolyte washed and rinsed thoroughly several times with distilled water, cleaned using acetone, dried and reweighed on a digital balance with a sensitivity of 0.001 g after every 24, 48 and 72 h. The weight loss was calculated as the difference in weight of the specimen before and after immersion in corrosion media (Mishra *et al.,* 2015). The corrosion rate (CR) in mg cm^{-2} h^{-1} was calculated from the following equation:

$$CR = \frac{\Delta W}{s \times t} \qquad (1)$$

Where ΔW is average weight loss, s is the total area of the specimen, and t is the immersion time. From the corrosion rate thus obtained, the inhibition efficiency (η %) was calculated as follows:

$$\eta\ \% = \frac{CR^\circ - CR}{CR^\circ} \times 100 \qquad (2)$$

Where CR° and CR are the corrosion rates of mild steel specimens in the absence and presence of inhibitor respectively.

Biological studies

Catalase-like activity

The catalase-like activity was observed by measuring the volume of O_2 produced during the reactions of the BENZONTHURA and complex 1-4 with H_2O_2 and compared with yeast catalase. The mini reactor is a Kitassato flask (100 cm^3) which was magnetically stirred and closed with a rubber septum and connected to a tank filled with water. This was arranged in a manner that the water will be pushed out as oxygen fills the tank. The volume of evolved dioxygen was measured for 14 min at two minute time intervals. In the first set of experiment, 5 mL yeast suspension in distilled water was added to the reactor through the septum. Thereafter, 20 mL aqueous solution of H_2O_2, (8 mmol, 30%) was injected into it through the rubber septum with a syringe. Similarly, 20 mL of H_2O_2 was added through the rubber septum with the help of a syringe to the 5 mL solution of BENZONTHURA and complex 1-4 in DMSO (1 mmol). The experiment was repeated for the highly efficient complex on different concentration. All the experiments were performed at room temperature at 25ºC (Pires *et al.*, 2013).

The velocity for the catalase-like activity of the complex 1 was obtained by time-dependent measurement of decomposition of hydrogen peroxide to water and evolved dioxygen.

In-vitro antibacterial screening

Ligand BENZONTHURA and complex 1-4 were screened for antibacterial activity against gram-negative bacteria *Escherichia coli*, (ATCC no. 35218) at different concentration. Agar well diffusion method was used for antibacterial screening as discussed earlier (Pelczar *et al.*, 2001). In order to observe the activity and confirm the sensitivity, BENZONTHURA, and complex 1-4 were tested for minimum inhibitory concentration (MIC). The most popular method for MIC evaluation, commonly used in the clinical laboratory is successive dilution method as discussed earlier (Mehrotra *et. al.*, 2015).

RESULTS AND DISCUSSION

Characterization of ligand

The empirical formula of BENZONTHURA was in agreement with elemental analysis. The ESI-MS of BENZONTHURA (Figure 1) shows peaks at m/z: 108.0340, 211.0762, 255.0807, 358.1068 and 447.57 were attributed for $[C_7H_7O + H^+]^+$, $[C_{14}H_{12}NO + H^+]^+$, $[C_{15}H_{21}NOS + H^+]^+$, $[C_{22}H_{17}N_2OS + H^+]^+$, and $[C_{29}H_{23}N_2OS]^+$ respectively. The peak at 465.1680 was attributed to pseudo molecular ion $[C_{29}H_{24}N_2O_2S + H^+]^+$.

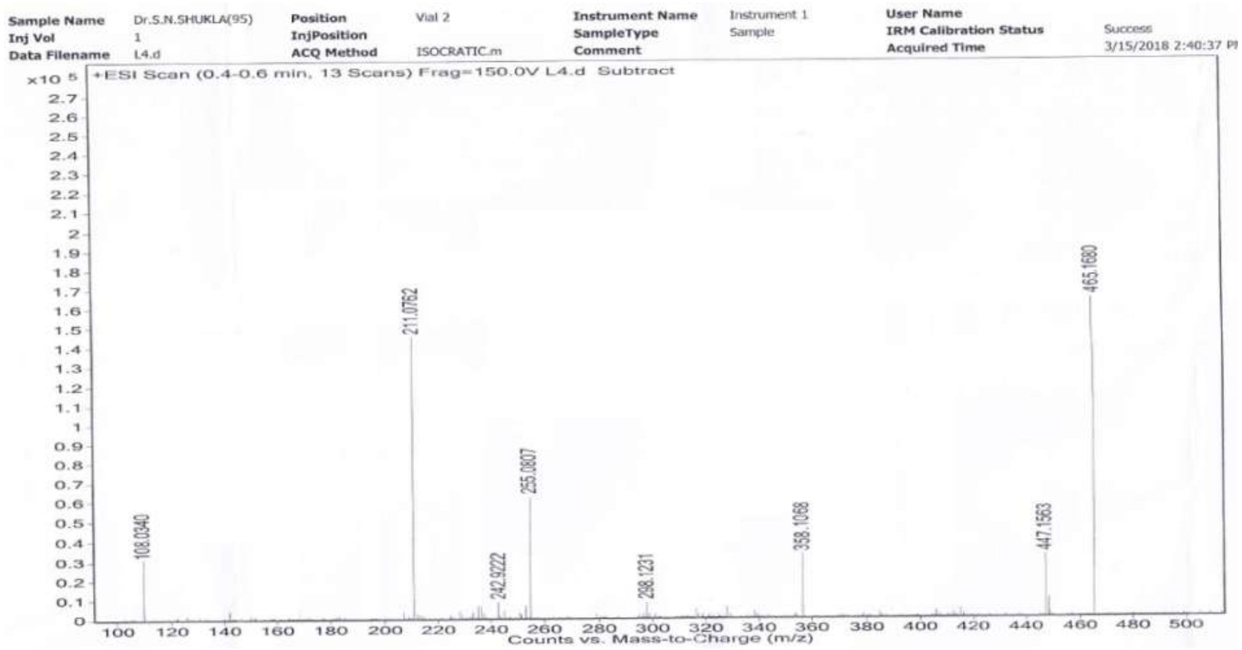

Figure 1: ESI-Mass of Ligand BENZONTHURA

FT-IR spectra of BENZONTHURA (Figure 2) exhibit a peak at 3282 cm^{-1} probably due to hydrogen bonding, attributed to hydroxyl ν(O-H) stretching vibration. Few peaks of medium intensity at ~1602 cm^{-}

^{1} attributed to the stretching vibrations of the ν(C=N) imine group. A peak appears at 1255 cm^{-1} which are assigned for phenolic ν(C-O) group. It also exhibits a signal of sharp intensity at 773 cm^{-1} attributed to ν(C=S) stretching vibrations (Silverstein *et. al.*, 1991).

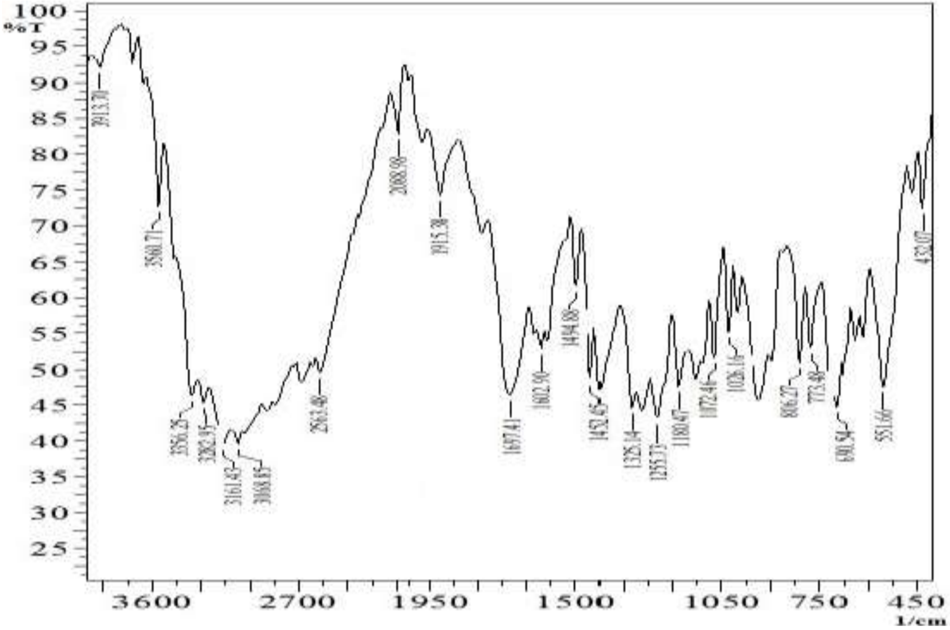

Figure 2: FT-IR spectra of BENZONTHURA

UV–Vis spectra of **BENZONTHURA** (Figure 3) exhibit two absorption bands at about 240 nm and 320 nm. The band of medium intensity at 240 nm was assigned to the intra-ligand n→ π* transition for (C=N) imine nitrogen. The strong band at 320 nm was attributed to π→ π* transition associated with aromatic ring.

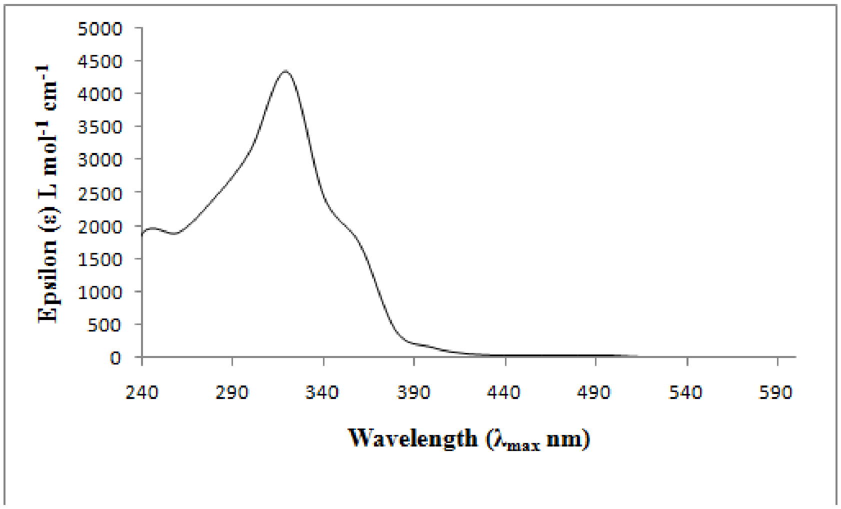

Figure 3: UV-Vis spectra of BENZONTHURA

^{1}H-NMR spectra of **BENZONTHURA** (Figure 4) displayed twelve triplets and eight doublets in aromatic region. Doublets centered at δ 7.280, δ 7.317, δ 7.335, δ 7.338, δ 7.910, δ 7.973, δ 7.976 and δ 7.981 ppm were attributed to 1H each for 8 protons. However, twelve triplets centered at δ 7.198, δ 7.235, δ 7.241, δ 7.346, δ 7.402, δ 7.420, δ 7.424, δ 7.439, δ 7.459, δ 7.475, δ 7.531 and δ 7.534 ppm were assigned for 1H each for twelve proton. A doublet centered at δ 6.983 ppm was attributed to two OH protons. Two singlets observed at δ 2.509 and δ 2.505 ppm were attributed for –CH protons.

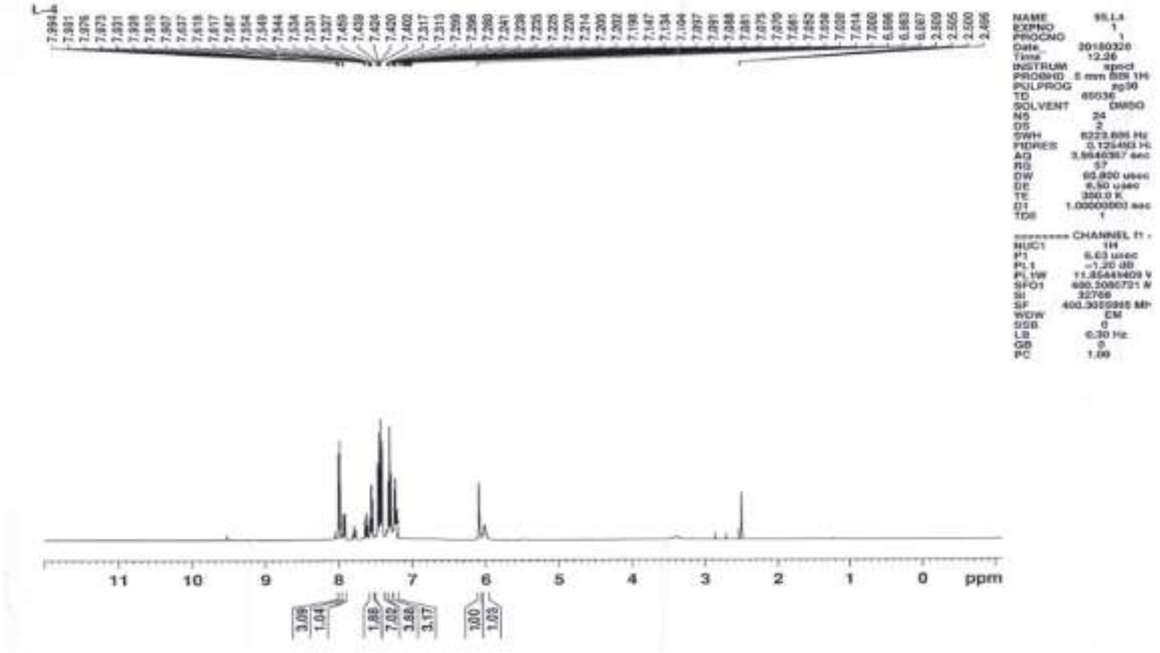

Figure 4: ^{1}H-NMR spectra of BENZONTHURA

^{13}C-NMR spectrum of BENZONTHURA (Figure 5) exhibit a signal at δ 199.21 ppm attributed for thione (C=S) carbon and also a signal at δ 183.88 ppm assigned for imine (C=N) carbon. The signal appeared at δ 164.85 ppm was attributed to the carbon linked with hydroxyl group. All aromatic carbon display signals in between δ 126.93-139.70 ppm.

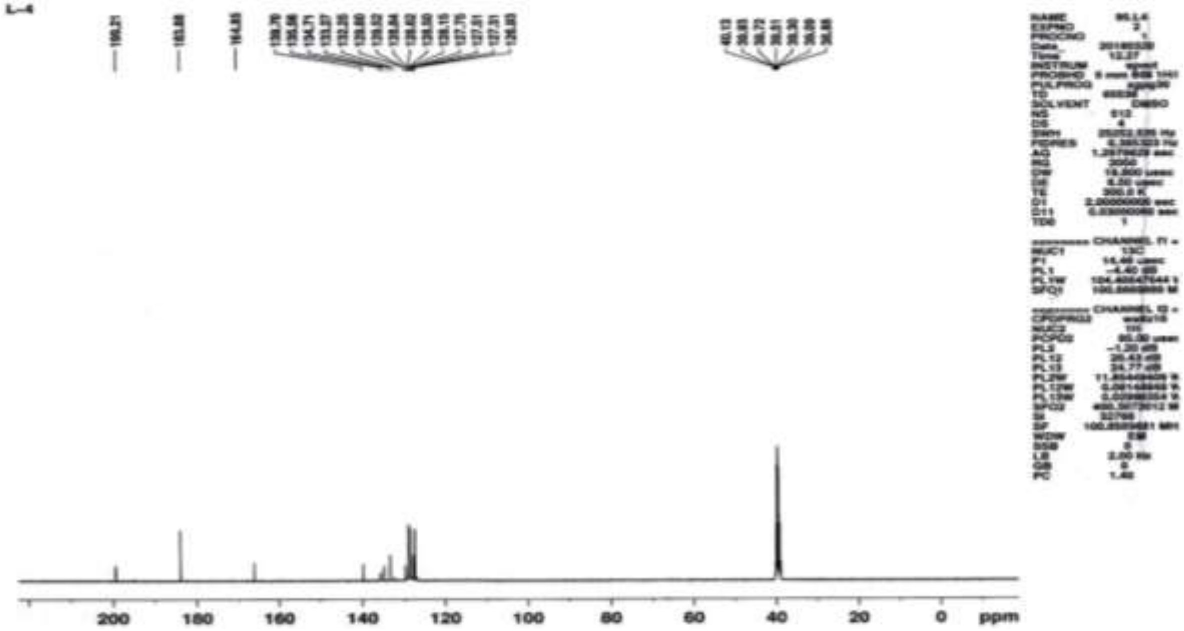

Figure 5: ^{13}C-NMR spectra of BENZONTHURA

Thus, on the basis of the elemental analysis, ESI-MS, UV-Vis, FT-IR, ^{1}H-NMR and ^{13}C-NMR spectra the probable structure of BENZONTHURA is suggested in Figure 6.

Research Article

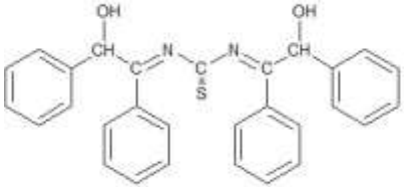

Figure 6: Structure of BENZONTHURA

Characterization of Complexes

The stoichiometries of the complexes were in agreement with elemental analyses. Molar conductance of complex 1-4 was between 11-16 $\Omega^{-1}cm^2mol^{-1}$ indicative of their non ionic nature (Geary, 1971). In ESI-MS of complex 1 peaks at m/z 210.1186, 344.2077, 465.2447, 518.3091 and 536.0970 were attributed for $[C_{14}H_{11}NO + H^+]^+$, $[C_{15}H_{15}MnNO_3S]^+$, $[C_{29}H_{22}N_2O_2S + 3H^+]^+$, $[C_{29}H_{22}MnN_2O_2S + H^+]^+$, and $[C_{29}H_{24}MnN_2O_2S + H^+]^+$ respectively. The pseudomolecular ion peak at m/z 554.1057 was attributed to $[C_{29}H_{26}MnN_2O_4S + H^+]^+$. In complex 2 peaks were observed at m/z 210.1545, 361.9715, 465.1456, 519.0891, 537.0866 and 554.0441were attributed for $[C_{14}H_{11}NO + H^+]^+$, $[C_{15}H_{13}FeNO_2SCl]^+$, $[C_{29}H_{22}N_2O_2S + 3H^+]^+$, $[C_{29}H_{22}FeN_2O_2S+ H^+]^+$, $[C_{29}H_{24}FeN_2O_3S+ H^+]^+$ and $[C_{29}H_{22}FeN_2O_2SCl+ H^+]^+$ respectively. Also a peak at m/z 572.0569 was pseudomolecular ion peak for $[C_{29}H_{24}FeN_2O_3SCl + H^+]^+$. In complex **3** exhibit several peaks at m/z 210.0909, 348.0156, 465.0466, 522.0812 and 540.0812 were attributed for $[C_{14}H_{11}NO + H^+]^+$, $[C_{15}H_{15}CoNO_3S]^+$, $[C_{29}H_{22}N_2O_2S + 3H^+]^+$, $[C_{29}H_{22}CoN_2O_2S + H^+]^+$, $[C_{29}H_{24}CoN_2O_3S + H^+]^+$. Also, a peak at 558.0963 was due to pseudomolecular ion $[C_{29}H_{26}CoN_2O_4S + H^+]^+$. Complex 4 shows peak at, m/z 210.0912, 347.0150, 465.1450, 521.0722 and 539.0925 attributed for $[C_{14}H_{11}NO + H^+]^+$, $[C_{15}H_{15}NiNO_3S]^+$, $[C_{29}H_{22}N_2O_2S + 3H^+]^+$, $[C_{29}H_{22}NiN_2O_2S + H^+]^+$ and $[C_{29}H_{24}NiN_2O_3S + H^+]^+$. Also a peak at m/z 558.0860 was due to pseudomolecular ion $[C_{29}H_{26}NiN_2O_4S + H^+]^+$. ESI-MS of complex 1 is shown in Figure 7.

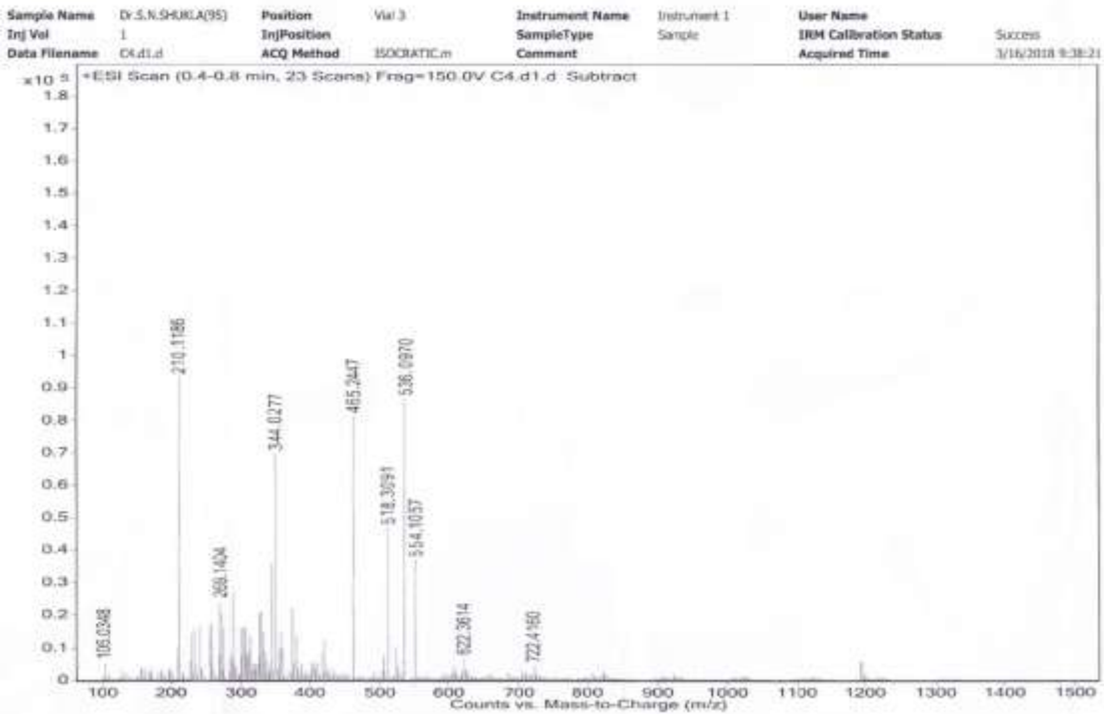

Figure 7: ESI-MS spectra of complex 1

In FT-IR spectra of BENZONTHURA, a strong peak appeared at 1602 cm^{-1} for imine ν(C=N) group was shifted downwards in the complexes and observed in between 1578-1586 cm^{-1} indicating the coordination of imine nitrogen to the metal. This was also supported by the appearance of new sharp signals between 460-476 cm^{-1} in the complexes due to M-N coordination. A sharp peak appeared at 3282 cm^{-1} in BENZONTHURA assigned to O-H stretching was vanished completely in the complexes and a new peak was appeared in between 580-589 cm^{-1} was assigned to M-O stretching indicative of the bonding of metal to the oxygen by removal of phenolic hydrogen. A peak at 1255 cm^{-1} in BENZONTHURA assigned to phenolic ν(C-O) stretching was moved to a higher in complex 1-4 and appeared in between 1290-1325 cm^{-1} confirming coordination of phenolic oxygen with metal. (Canpolat *et. al.*, 2005). All complexes shows a peak in between 830-838 cm^{-1} may be due to wagging vibration of coordinated water. BENZONTHURA exhibits a sharp signal at 773 cm^{-1} for ν(C=S) group was shifted downwards in the complexes and observed in between 751-758 cm^{-1} indicating the coordination of sulphur to the metal. Complex 2 shows a peak at 403 cm^{-1} which was probably due to Fe-Cl bond. FT-IR spectra of complex 1 is given in Figure 8**.**

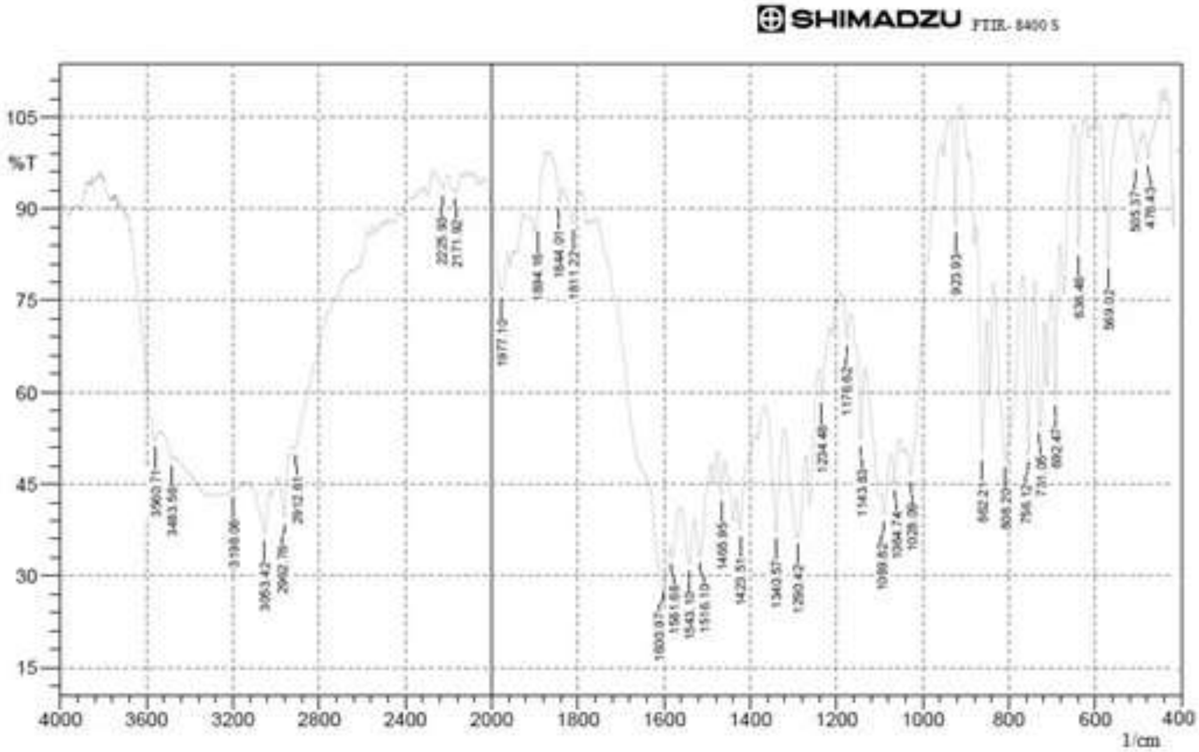

Figure 8: FT-IR spectra of complex 1

The free ligand exhibited two strong absorptions bands at 240 and 320 nm which was due $\pi \rightarrow \pi^*$ and $n \rightarrow \pi^*$ transitions. In complexes absorption band in the range between 220-240 nm and 340-380 nm were attributed to $\pi \rightarrow \pi^*$ and $n \rightarrow \pi^*$ transition associated with (C=N) imine nitrogen and intra ligand charge transfer respectively. The bathochromic shift of this absorption upon complexation was due to the donation of a lone pair of electrons to the metal ion, indicating the coordination of imine nitrogen. These transitions were shifting to higher or lower frequencies might be due to the ligand to metal and metal to ligand charge transfer.

Complex **1** exhibits magnetic moment of 5.27 B.M. which indicate that complex was high spin with five unpaired electrons in Mn(II). It shows three absorption bands at 720 nm, 640 nm, and 580 nm attributed to $^6A_{1g} \rightarrow {}^4T_{1g}(\nu_3)$, $^6A_{1g} \rightarrow {}^4T_{2g}(\nu_2)$ and $^6A_{1g} \rightarrow {}^4E_g$, $^4A_{1g}(\nu_1)$ transitions respectively, indicating distorted octahedral geometry around Mn(II) ion (Figure 9). Complex **2** exhibits magnetic moment of 5.59 B.M., which is due to the presence of five unpaired electrons and high spin octahedral arrangement. Complex **2** shows two bands at 720 nm and 520 nm attributed to $^6A_{1g} \rightarrow {}^4T_{2g}(\nu_3)$ and $^6A_{1g} \rightarrow {}^4T_1(\nu_2)$ respectively, indicates an octahedral geometry around the metal ion and rest three band at 480 nm, 340 nm and 220 nm are due to charge transfer, n→ π* and π→ π* transitions respectively. The magnetic moment of complex **3** was 4.02 B.M. corresponding to three unpaired electrons in Co (II). The electronic spectrum of this complex exhibit three bands at 788, 740 and 550 nm which may be assigned to the $^4T_{1g}(F) \rightarrow {}^4T_{2g}(\nu_1)$, $^4T_{1g}(F) \rightarrow {}^4A_{2g}(\nu_2)$ and $^4T_{1g} \rightarrow {}^4T_{1g}(\nu_3)$ transition confirming an octahedral geometry. Complex **4** exhibit magnetic susceptibility of 2.99 B.M., indicating the presence of two unpaired electrons in Ni(II) ion consistent with octahedral geometry. The electronic spectrum of complex **4** displayed two bands at 580 nm and 420 nm assigned for $^3A_{2g} \rightarrow {}^3T_{1g}(\nu_2)$ and $^3A_{1g} \rightarrow {}^3T_{1g}(\nu_3)$ d–d transitions indicative of Ni(II) ion in an octahedral environment (Singh, 1980).

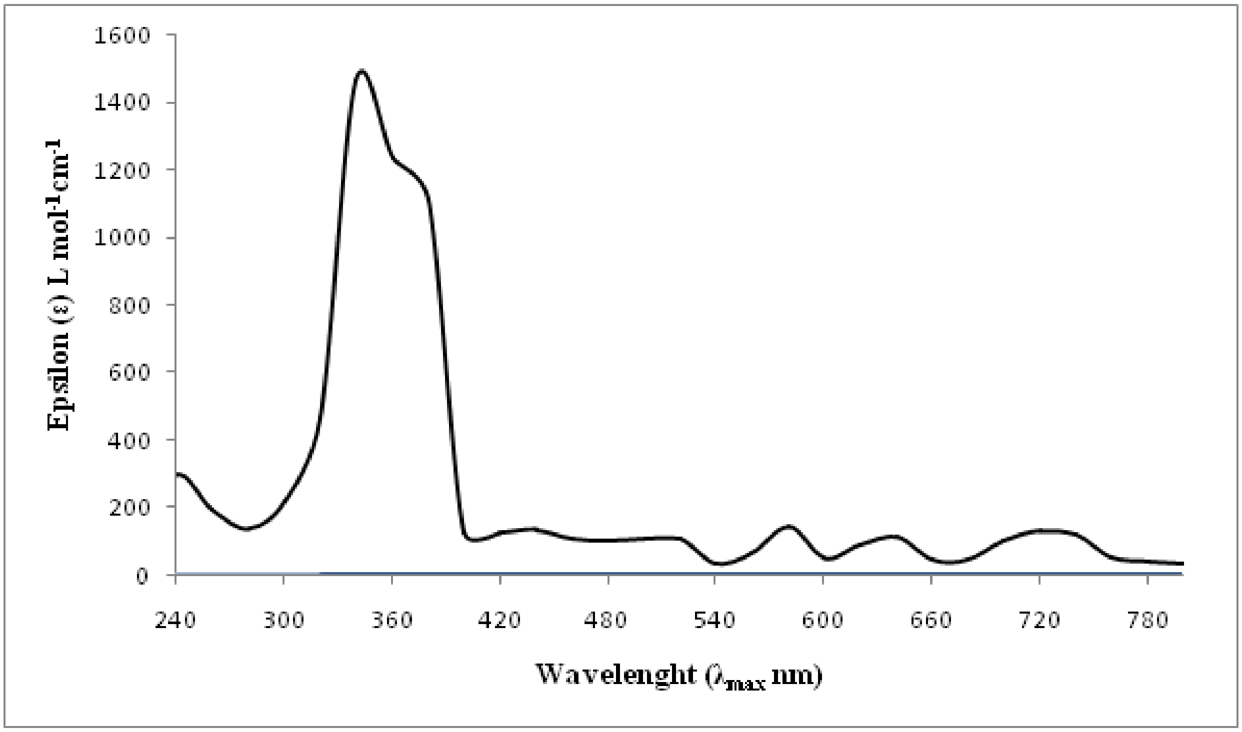

Figure 9: UV-Vis spectra of complex 1

Geometry optimization

Quantum chemical parameters

The assertion of energies of the HOMO and LUMO is the essential norm in quantum estimations. The HOMO "Highest Occupied Molecular Orbital" is the one, which principally behaves as an electron donor. On the other hand, the LUMO "Lowest Unoccupied Molecular Orbital" is the orbital that greatly behaves as the electron receiver. These orbitals were named as frontier molecular orbital (FMOs). The E_{HOMO}, E_{LUMO} and the adjoining levels are practically negative. This illustrates the stability of the isolated chelate. The energy gap ($\Delta E = (E_{\mathrm{LUMO}}) - (E_{\mathrm{HOMO}})$) is a critical indicator that describes the chemical reactivity and kinetic stability of the investigated material. The calculated values of the following quantum chemical parameters: Difference between HOMO and LUMO energy levels (ΔE), Mulliken electronegativity (χ), absolute hardness (η), absolute softness (σ), chemical potential (Pi), global softness (S), global electrophilicity (ω), additional electronic charge (ΔN_{max}), dipole moment (μ) and total energy E (RB3LYP) after geometrical optimization of the structures of compounds were listed in Table 1.

$$\chi = -1/2\ (E_{LUMO} + E_{HOMO}) \qquad (1)$$

$$\eta = 1/2\ (E_{LUMO} - E_{HOMO}) \qquad (2)$$

$$\sigma = 1/\eta \qquad (3)$$

$$Pi = -\chi = 1/2\ (E_{LUMO} + E_{HOMO}) \qquad (4)$$

$$S = 1/2\ \eta \qquad (5)$$

$$\omega = Pi^2/2\ \eta \qquad (6)$$

$$\Delta N_{max} = -Pi/\ \eta \qquad (7)$$

In the compounds under investigation, some important molecular orbitals for the BENZONTHURA and the complex 1 were selected to explain the difference that occurred to the various energy characters of BENZONTHURA when bonded with metal. BENZONTHURA coordinates to metal ions through the nitrogen of imine, deprotonated oxygen of the hydroxyl group and sulfur of thione group. These atoms carry more charge confirming active sites for coordination. The energy difference between values of absolute softness (σ) in BENZONTHURA and complex 1 indicates that BENZONTHURA has a good tendency to chelate with metal ions. The negative values of chemical potential (*Pi*) in complex **1** indicate that energy must decrease upon accepting electronic charge form BENZONTHURA. The value of *Pi* depends upon the Mulliken electronegativity (χ). The increase in the global electrophilicity (ω) value of complex 1 attributed to higher electron accepting capability (Parr *et al.*, 1999).

Table 1: Calculated quantum chemical parameters of BENZONTHURA and complex 1

Ligand / Complex	E_{HOMO} (eV)	E_{LUMO} (eV)	ΔE (eV)	χ (eV)	η (eV)	σ (eV^{-1})	Pi (eV)	S (eV^{-1})	ω (eV)	ΔN_{max} (eV)	Total energy (a.u.)	Dipole moment (Debye)
BENZONTHURA	-4.061	-2.782	1.279	3.421	0.639	1.563	-3.421	0.781	9.152	5.350	-1777.140	5.690
Complex 1 (α)	-5.183	-2.620	2.563	3.901	1.281	0.780	-3.901	0.390	5.939	3.044	-1644.708	3.478
Complex 1 (β)	-4.291	-1.855	2.436	3.073	1.218	0.821	-3.073	0.410	3.876	2.522		

Charge population analysis and electron density plots

Mulliken atomic charge computation and natural charge population analyses of natural bond orbital (NBO) have a noteworthy part in the use of quantum chemical estimation to the molecular framework on account of atomic charges impact, electronic structure, molecular polarizability, dipole moment and other properties of the framework (Mulliken, 1955). The comparative values of both scales for BENZONTHURA and complex 1 are recorded in Table 2. The S, O and N atoms revealed a negative charge because of their donating property. Moreover, S and O atoms have bigger ones more than N atoms. Hydrogen atoms of BENZONTHURA and metal atom of complex 1 display positive charges because of their accepting property. Charge distribution on each atom of BENZONTHURA and complex **1** is shown in Figure 10 (a), (b), (c), and (d).

Table 2: Selected Mulliken atomic charges and NBO partial charges of BENZONTHURA and complex 1

S. No.	Bond Connectivity	BENZONTHURA			Complex1		
		Atom	**Mulliken Charges**	**Natural Charges**	**Atom**	**Mulliken Charges**	**Natural Charges**
1.	C (connected with O)	C2	0.150	0.083	C2	-0.227	0.090
2.	C (connected with O′)	C3	0.108	0.084	C3	-0.195	0.088
3.	C (connected to imine N)	C28	0.182	0.183	C17	0.058	0.290
4.	C (connected to imine N′)	C29	0.159	0.121	C18	0.101	0.326
5.	C (connected with S)	C58	-0.036	-0.172	C45	-0.152	0.168
6.	H (connected to O)	H55	0.317	0.495	-	-	-
7.	H (connected to O′)	H56	0.312	0.482	-	-	-
8.	O	O1	-0.539	-0.755	O1	-0.490	-0.726
9.	O′	O43	-0.529	-0.734	O32	-0.413	-0.654
10.	H1 (connected to hydroxyl O)	-	-	-	H60	0.444	0.539
11.	H2 (connected to hydroxyl O)	-	-	-	H61	0.415	0.515
12.	H1 (connected to hudroxyl O′)	-	-	-	H62	0.456	0.539
13.	H1 (connected to hudroxyl O′)	-	-	-	H63	0.444	0.547
14.	O (hydroxyl)	-	-	-	O58	-0.607	-0.787
15.	O′ (hydroxyl)	-	-	-	O59	-0.680	-0.793
16.	N(imine)	N30	-0.463	-0.420	N19	-0.232	-0.485
17.	N′(imine)	N31	-0.408	-0.381	N20	-0.230	-0.479
18.	S	S57	-0.335	-0.500	S44	-0.096	-0.055
19.	Mn	-	-	-	Mn46	0.574	0.543

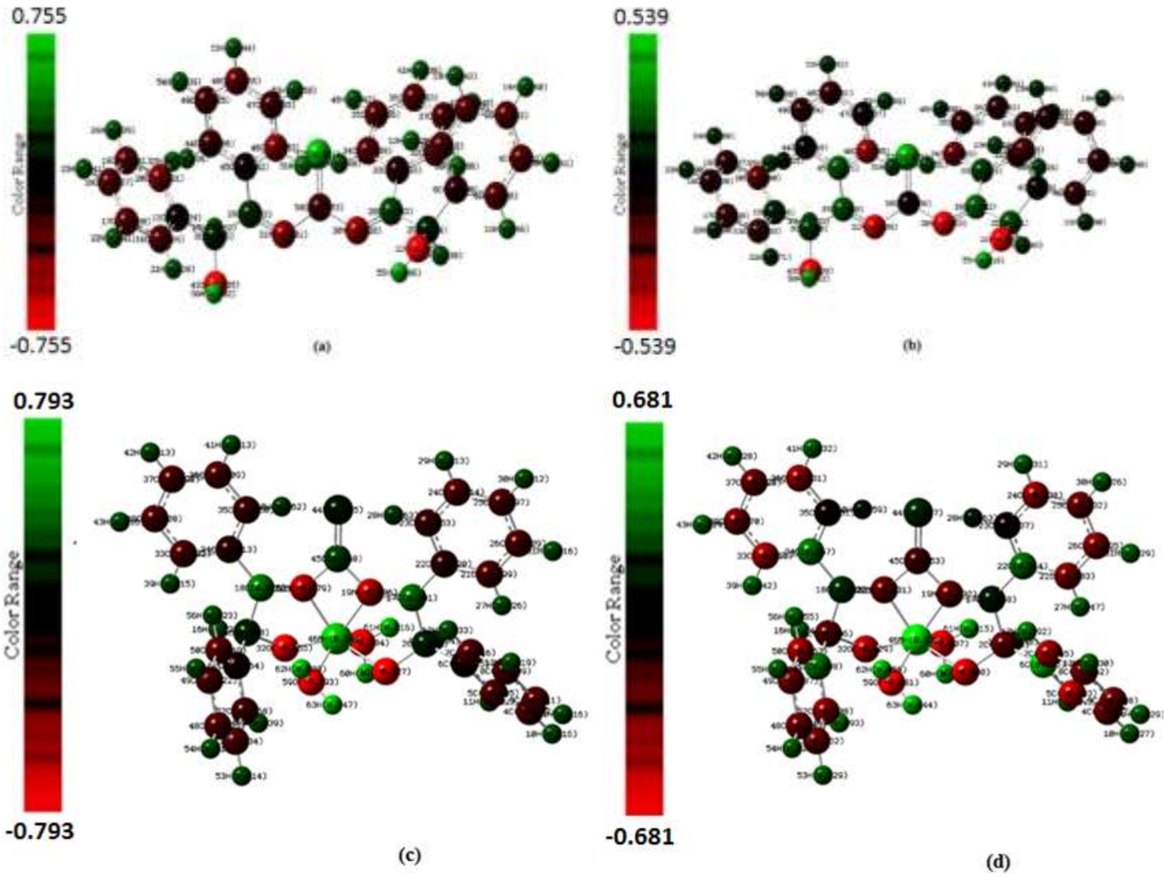

Figure 10: (a) Natural atomic charges of BENZONTHURA, (b) Mulliken atomic charges of BENZONTHURA, (c) Natural atomic charges of complex 1, (d) Mulliken atomic charges of complex 1

Molecular electrostatic potential analysis (MEP) maps

The MEP is defined as an electrostatic potential charted onto the stationary electron density surface. MEP is likewise extremely accommodating in research of the structure with its physio-chemical relationship and also hydrogen bonding collaborations. As it can be easily observed from the MEP map of the ligand, greatest negative area favored for the electrophilic reaction is shown by the red color, while the extreme positive district favored for the nucleophilic reaction is illustrated by the blue color. The increase in the potential can be ordered as follow: blue > green > red, where blue demonstrates the powerful attraction while the red illustrates the powerful repulsion. Areas with negative values are distributed on nitrogen, oxygen and sulfur atoms while the regions having the positive values are distributed on the hydrogen

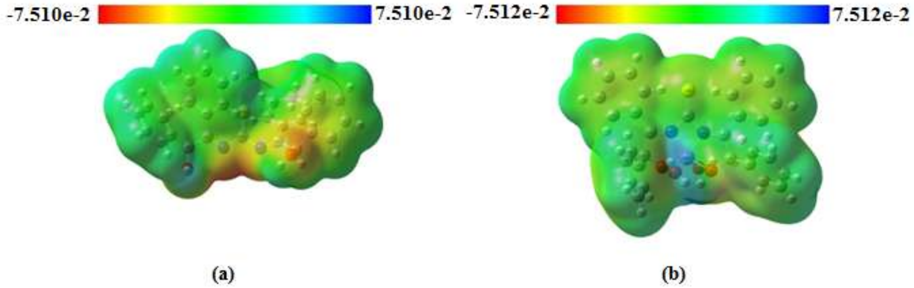

Figure 11: Molecular Electrostatic Potential map (MEP) of (a) BENZONTHURA, and (b) complex 1

atoms and the metal atom (Scrocco et al., 1978). The "MEP" maps of BENZONTHURA and its complex 1 are shown in Figure 11 (a) and (b).

Thus, on the basis of the elemental analysis, ESI-MS, molar conductance, magnetic susceptibility, electronic spectra, FT-IR, ^{1}H-NMR, ^{13}C-NMR and DFT studies, the probable structure of the BENZONTHURA and complex 1-4 were suggested as below in Figure 12 (a-f).

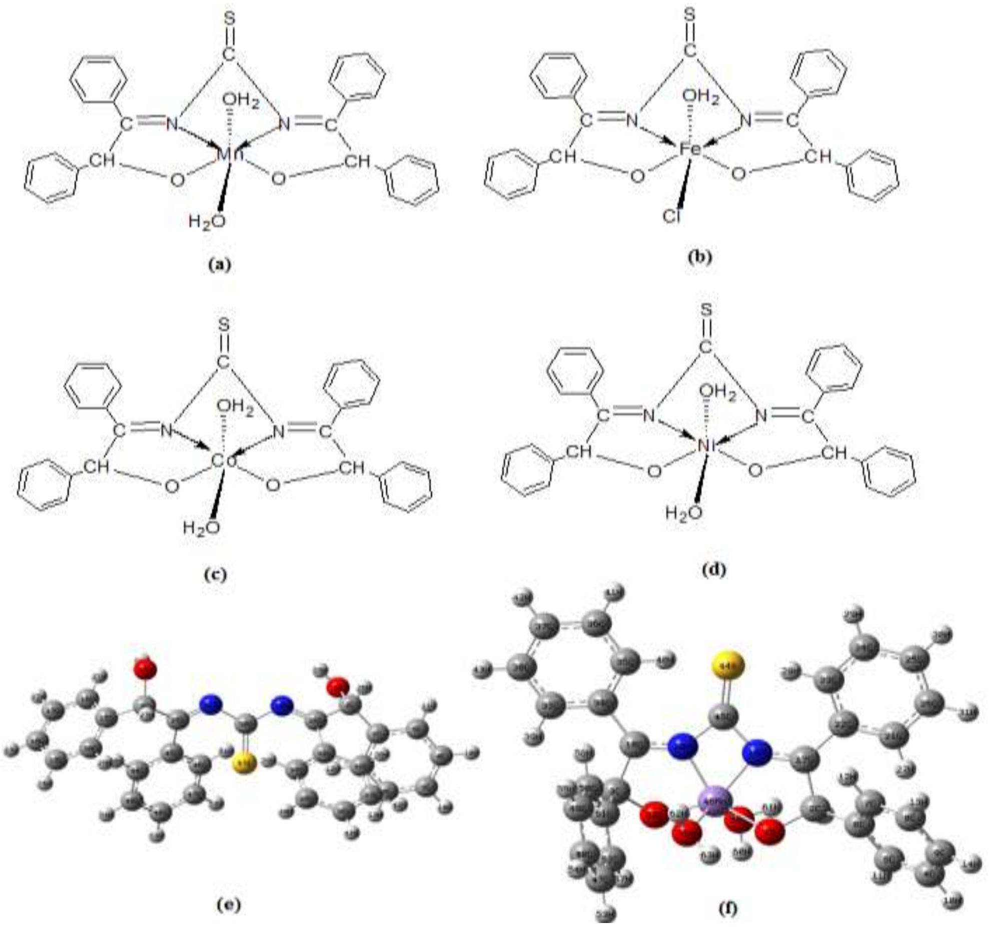

Figure 12: ChemDraw structure of (a) complex 1, (b) complex 2, (c) complex 3, (d) complex 4, DFT optimized structure of (e) BENZONTHURA, and (f) complex 1

Corrosion inhibition efficiency

Weight loss measurement

Corrosion inhibition study of ligand BENZONTHURA and complexes 1-4 was performed by using weight loss measurement method. The concentration of the ligand BENZONTHURA and their complexes 1-4 were chosen to be each 50 ppm. It was observed that ligand BENZONTHURA exhibits better corrosion inhibition efficiency than complex 1-4. This difference in inhibition efficiency was because of the presence of N, O and S atom in BENZONTHURA, which increases electron density to a greater extent as compared to complexes. The results show that better adsorption of BENZONTHURA and complex 1-4 on the corroding surface. Interestingly, complex 2 containing Fe(III) metal ion shows much lower efficiencies than the other complexes, this may be attributed to the fact that in case of iron complex, iron itself forms a layer over a corroding surface thus instead of inhibition it itself get corroded. It is apparent that corrosion rate decrease as time passes and corrosion inhibition efficiency increased with time (Moretti *et. al*., 2013). Corrosion parameters namely, corrosion rate (CR) and corrosion inhibition efficiency (η%) were calculated and shown in Table 3. A comparative corrosion rate and corrosion efficiency data of all the compounds were presented in Figure 13 (a) and (b). Corrosion inhibition efficiency rate follows the order **BENZONTHURA > 4 > 3 > 1 > 2**. Corrosion inhibition efficiency of complex **4** was quite higher than other complexes and slightly smaller than ligand BENZONTHURA.

Table 3: Corrosion parameters of mild steel in HCl solution in the presence and absence of inhibitor at a different time interval, obtained from weight loss measurements

Ligand/Complexes	Corrosion Rate (mg cm^{-2} h^{-1})			Corrosion inhibition efficiency η %		
	24 h	**48 h**	**72 h**	**24 h**	**48 h**	**72 h**
BENZONTHURA	15.20	8.40	6.80	59.06	77.38	81.68
Complex 1	22.77	12.70	11.94	38.27	65.79	67.85
Complex 2	24.79	18.12	13.24	33.27	51.21	64.36
Complex 3	20.13	11.28	8.45	45.79	66.25	72.22
Complex 4	16.45	9.86	7.45	55.70	73.45	76.41

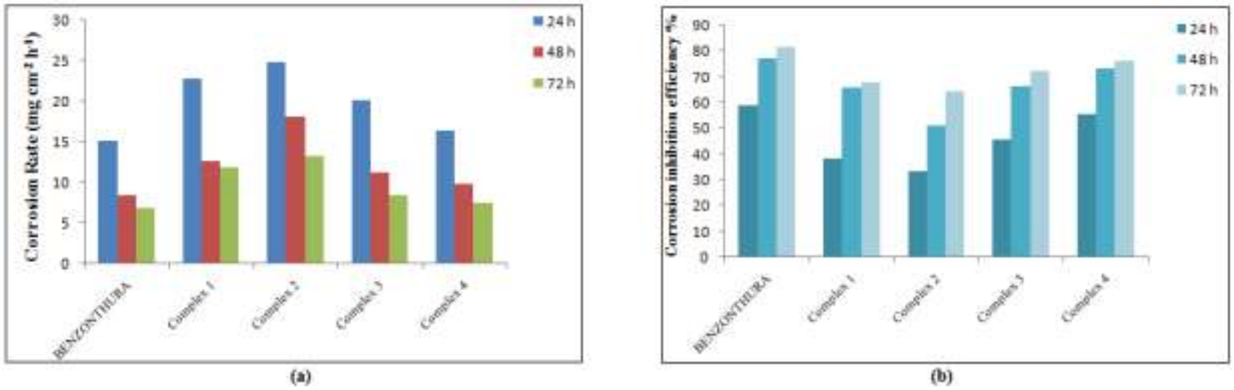

(a) (b)

Figure 13: (a) Corrosion rate of compounds, (b) Corrosion inhibition efficiency of compounds

Biological applications

Experimental study of in vitro catalase-like activity

The catalytic decomposition of H_2O_2 was shown by all metal complexes. Among them, complex 1 and complex 2 shows more effective catalytic efficiency than other complexes. Experiments were repeated many times to ensure constancy of the results. Volumetric measurements of the evolved O_2 shows that BENZONTHURA and complexes 1-4 are able to catalytically disproportionate H_2O_2 into H_2O and O_2. The experiment has been carried out by taking each compound (5 mL, 1 mmol in DMSO) in a Kitassato flask and adding 20 mL of 30 % H_2O_2 with the help of a syringe through a rubber septum. Immediately, after the addition of H_2O_2 in the compounds, decomposition of H_2O_2 starts and volume of dioxygen evolve is measured from a graduated burette. The complete reaction was monitored for 14 minute and amount of dioxygen evolved for BENZONTHURA and complex 1-4 are shown in Figure 14 (a). It was observed that catalase being a natural enzyme evolve 4.19×10^{-1} mol of dioxygen. In BENZONTHURA and complex 1-4, the amount of dioxygen evolves are 1.78×10^{-1}, 3.52×10^{-1}, 2.72×10^{-1}, 2.32×10^{-1} and 1.87×10^{-1} mol respectively. The progression profile of all complexes in Figure 14 shows the fast catalytic process of complex 1 as compared to the other synthesized complexes. The order of hydrogen peroxide decomposition is catalase > 1 > 2 > 3 > 4 > BENZONTHURA. Since the complex 1 exhibit highest evolved dioxygen, the initial rate of H_2O_2 disproportionation by complex 1 was calculated by the further experiment. The plot of evolving dioxygen against time for the different concentration of hydrogen peroxide is shown in Figure 14 (b). An experiment using 1 as catalyst in DMSO at 25^{o}C was also performed and after 14 min at $[\text{Complex } 1]_0 = 5 \times 10^{-3}$ mol dm^{-3} and $[H_2O_2]_0 = 2 \times 10^{-3}$, 3×10^{-3}, 5×10^{-3}, 8×10^{-3} mol dm^{-3} concentration, 3.21×10^{-4}, 3.75×10^{-4}, 4.87×10^{-4} and 6.20×10^{-4} mmol of dioxygen was evolved respectively.

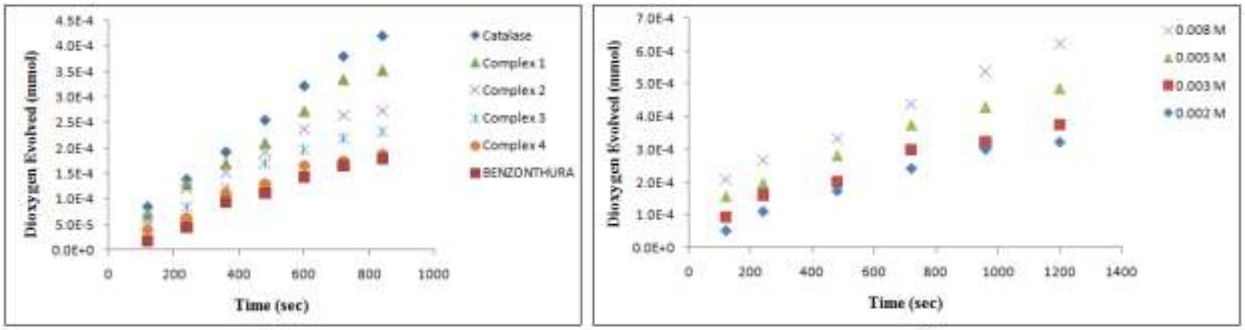

(a) (b)

Figure 14: (a) Dioxygen evolution (mmol) in the disproportionation of H_2O_2, (b) Dioxygen evolution (mmol) at different concentrations of H_2O_2

Antibacterial assessments

All the compounds showed considerable bactericidal activity against *E. coli*. The *in vitro* antibacterial activity of the BENZONTHURA and complex 1-4 were tested using the agar well diffusion method. Chelation of Schiff base with metal ion will enhance the lipophilicity of the central metal atom, which subsequently favors its permeation through the lipid layers of the cell membrane and blocking the metal binding sites on enzymes of microorganisms (Shukla *et al.*, 2015). The growth inhibition zone was measured in diameter (mm) and the results are listed in Table 4. All the tested compounds showed good antibacterial activity against the selected microorganism *E. coli*. The obtained results indicate that the complexes were more effective against *E. coli* under identical experimental conditions. Ni(II) complex has higher bacterial activity than the other complexes. The bioactivity of the BENZONTHURA and their complexes are found to order: **4 > 1 > 2 > 3 > BENZONTHURA.**

Minimum inhibitory concentration (MIC)

The MIC of the complexes and ligand is also displayed in Table 4. Since, the MIC is the concentration of the highest dilution tube, in which bacterial growth was absent. It was observed that complex 1-4 has exhibited MIC in between 0.45-0.51 µg/mL. It was also observed that the complex 4 was most active to inhibit bacteria with an inhibition zone of 33 mm and also the lowest minimum inhibitory concentration of 0.45 µg/mL MIC of the complexes follows the trend as **3 > 2 > 1 > 4.**

Table 4: Antibacterial screening data of BENZONTHURA and complex 1-4 against *E. coli*

S. No.	Ligands/Complexes	Diameter of inhibition zone (in mm)	MIC (µg/mL)
1	BENZONTHURA	20±1.2	-
2	Complex 1	31±0.9	0.48
3	Complex 2	27±0.5	0.50
4	Complex 3	25±0.8	0.51
5	Complex 4	33±1.2	0.45

**Values as mean ±Standard Error Mean.*

Conclusion

One novel ligand **BENZONTHURA** and its four with Mn(II), Fe(III), Co(II) and Ni(II) were synthesized. The geometries of the complexes were characterized by various spectroscopic methods and optimized by DFT calculations. The corrosion inhibition behaviors of ligand and complexes have been studied on mild steel in acidic medium. Ligand and complex **4** exhibits good anticorrosive activity. The synthesized compounds were also tested as catalysts for H_2O_2 decomposition. Complex **1** in solution mimic like catalase in disproportionation reaction of H_2O_2. Antibacterial activity of ligand and complexes indicate that activity of the ligand become more pronounced when coordinated with the metal ions. Hence, from all these extensive studies, it may be concluded that some of these complexes could be exploited for the design of novel anticorrosive material, antibacterial drug as well as catalytic material for scavenging peroxide formed in the biological system.

ACKNOWLEDGMENT

The authors are grateful to Principal Government Science College, Jabalpur and Head, Department of Chemistry for providing necessary laboratory facilities. We sincerely thanks SAIF-CDRI Lucknow, for recording elemental analysis, ESI- MS, ^{1}H-NMR, ^{13}C-NMR. One of us (Preeti Vaidya) is also grateful to the UGC-New Delhi for financial support through RGNF (Award letter no. F1-17.1/2015-16/RGNF-2015-17-SC-MAD-13266/(SAIII/Website)).

REFERENCES

Arslan H, Duran N, Borekci G, KorayOzer C and Akbay C (2009). Antimicrobial activity of some thiourea derivatives and their nickel and copper complexes. *Molecules* **14** 519-527.

Barone V, Mennucci B, Petersson G A, Nakatsuji H, Caricato M and LiX (2009). Gaussian 09, Revision D.01, Gaussian Inc. (Wallingford CT).

Becke AD (1988). Density-functional exchange-energy approximation with correct asymptotic behavior. *Physical Review A* **38(6)** 3098-3100.

Bielenica A, Stefańska J, Stępień K, Napiórkowska A, AugustynowiczKopeć E, Sanna G, Madeddu S, Boi S, Giliberti G, Wrzosek M and Struga M (2015). Synthesis, cytotoxicity, and antimicrobial of thiourea derivatives incorporating 3-(trifluoromethyl)phenyl moiety. *European Journal of Medicinal Chemistry* **101** 111-25.

Brazier MW, Doctrow SR, Masters CL and Collins SJ (2008). A manganese-superoxide dismutase/catalase mimetic extends survival in a mouse model of human prion disease. *Free Radical Biology and Medicine* **45(2)** 184-192.

Canpolat E and Kaya M (2005). Studies on Mononuclear Chelates Derived from Substituted Schiff Base Ligands (Part 4): Synthesis and Characterization of a New 5-Hydroxysalicyliden-*P*-Aminoacetophenoneoxime and Its Complexes with Co(II), Ni(II), Cu(II) and Zn(II). *Turkish journal of chemistry* **29** 409-415.

Collin B, Busseuil D, Zeller M, Perrin C, Barthez O and Duvillard L (2007). Increased superoxide anion production is associated with early atherosclerosis and cardiovascular dysfunctions in a rabbit model. *Molecular and Cellular Biochemistry* **294(1-2)** 225-235.

Fox RB, Harada RN, Tate RM and Repine JE (1993). Dimethylthiourea protects rats against gram-negative sepsis and decreases tumor necrosis factor and nuclear factor κB activity. *Journal of Applied Physiology* **129(4) 470-481.**

Frisch MJ, Trucks GW, Schlegel HB, Scuseria GE, Robb MA, Cheeseman JR, Scalmani G, Lee C, Yang W and Parr RG (1988). Development of the Colic-Salvetti correlation-energy formula into a functional of the electron density. *Physical Review B* **37(2)**, 785-789.

Geary WJ (1971). The use of conductivity measurements in organic solvents for the characterization of coordination compounds. *Coordination Chemistry Reviews* **7(1)** 81-122.

Guo L, Kaya S, Obot IB, Zheng X and Qiang Y (2017). Toward understanding the anticorrosive mechanism of some thiourea derivatives for carbon steel corrosion: A combined DFT and molecular dynamics investigation. *Journal of Colloid and Interface Science* **506** 478-485.

Halliwell BH and Gutteridge JMC (1984). Oxygen toxicity, oxygen radicals, transition metals and disease. *Biochemical Journal* **219(1)** 1-14.

Jeffery GH, Bassett J, Mendham J and Denney RC (1989). Vogel's Textbook of Quantitative Inorganic Analysis, 5th edn, (John Wiley & Sons, Inc, New York) 454-462.

Kadiiska MB, Mason RP, Dreher KL, Costa DL and Ghio AJ (1997). *In Vivo* Evidence of Free Radical Formation in the Rat Lung after Exposure to an Emission Source Air Pollution Particle. *Chemical Research in Toxicology* **10(10)** 1104-1108.

Lai Y-L, Wu H-D and Chen C-F (1998). Antioxidants Attenuate Chronic Hypoxic Pulmonary Hypertension. *Journal of Cardiovascular Pharmacology* **32(5)** 714-720.

Mehrotra R, Shukla SN and Gaur P (2015). Synthesis and spectroscopic characterization of antibacterial rhodium and ruthenium organometallics molded by C–H activation at the ortho position of a phenyl ring. *Journal of Coordination Chemistry* **68(4)** 650-661.

Mishra M, Tiwari K, Mourya P, Singh MM and Singh VP (2015). Synthesis, characterization and corrosion inhibition property of nickel(II) and copper(II) complexes with some acylhydrazine Schiff bases. *Polyhedron* **89** 29–38.

Moretti G, Guidi F and Fabris F (2013). Corrosion inhibition of the mild steel in 0.5 M HCl by 2-butyl-hexahydropyrrolo[1,2-b][1,2]oxazole. *Corrosion Science* **76** 206-218.

Mulliken RS (1955). Electronic Population Analysis on LCAO-MO Molecular Wave Functions. *Journal of Chemical Physics* **23(10)** 1833-1840.

Parr RG, Szentpaly Lv and Liu S (1999). Electrophilicity index. *Journal of the American Chemical Society* **121** 1922-1924.

Pelczar MJ, Chan ECS and Krieg NR (2001). *Text Book of Microbiology*, 5th edn (McGraw-Hill Publishing Company Ltd) New Delhi, India 138.

Pires BM, Silva DM, Visentin LC, Drago V, Carvalho NMF, Faria RB and Antunes OAC (2013). Synthesis, characterization and catalase-like activity of the tetranuclear iron(III) complex involving a (μ-oxo)(μ-hydroxo)bis(μ-alkoxo)tetra(μ-carboxylato)tetrairon core. *Inorganica Chimica Acta* **407** 69-81.

Rauf MK, Zaib S, Talib A, Ebihara M, Badshah A, Bolte M and Iqbal J (2016). Solution-phase microwave assisted parallel synthesis, biological evaluation and in silico docking studies of *N,N′*-disubstituted thioureas derived from 3-chlorobenzoic acid. *Bioorganic & Medicinal Chemistry* **24(18)** 4452-4463.

Ray PS, Maulik G, Cordis GA, Bertelli AAE, Bertelli A and Das DK (1999). The red wine antioxidant resveratrol protects isolated rat hearts from ischemia reperfusion injury. Free Radical Biology and Medicine **27(1-2)** 160-169.

Scrocco E and Tomasi J (1978). Electronic Molecular Structure, Reactivity, and Intermolecular Forces: An Euristic Interpretation by Means of Electrostatic Molecular Potentials. in: *L. Per-Olov* (edn.), Vol 11, *Advances in Quantum Chemistry* (Academic Press) 115-193.

Shukla SN, Gaur P, Gupta JP, Mathews S and Rai N (2015). Synthesis, characterization and antibacterial activity of complexes of palladium with Schiff bases derived from 1, 3-diaminopropane. *International Journal of Basic and Applied Chemical Sciences* **5(1)** 18-28.

Silverstein RM, Bassler GC and Morrill TC (1991). Spectrometric Identification of Organic Compound. (John Wiley and Sons, Inc) New York 82-108, 123-131, 219-262.

Singh P, Singh AK and Singh VP (2013). Synthesis, structural and corrosion inhibition properties of some transition metal(II) complexes with *o*-hydroxyacetophenone-2-thiophenoyl hydrazone. *Polyhedron* **65** 73-81.

Singh PP (1980). Bimetallic Tetrathiocyanates and Selenocyanates as Lewis acids. *Coordination Chemistry Reviews* **32** 33-65.

Thannickal VJ and Fanburg BL (2000). Reactive oxygen species in cell signaling. *America Journal of Physiology Lung Cellular and Molecular Physiology* **279(6)** L1005-L1028.

Valdez CE, Smith QA, Nechay MR and Alexandrova AN (2014). Mysteries of Metals in Metalloenzymes. *Accounts of Chemical Research* **47(10)** 3110-3117.

Walpole C, Ko SY, Brown M, Beattie D, Campbell E, Dickenson F, Ewan S, Hughes GA, Lemaira M, Lerpiniere J, Patel S and Urban L (1998). 2-Nitrophenylcarbamoyl-(S)-prolyl-(S)-3-(2-naphthyl)alanyl-N-benzyl-Nmethylamide (SDZ NKT 343), a Potent Human NK1 Tachykinin Receptor Antagonist with Good Oral Analgesic Activity in Chronic Pain Models. *Journal of Medicinal Chemistry* **41** 3159-3173.

Zhang YM, Wei TB, Wang XC and Yang SY (1998). Synthesis and biological activity of N-aroyl-N'-carboxyalkyl thiourea derivatives. *Indian Journal of Chemistry -Section B* **37** 604-606.